Garnet sand reveals rock recycling processes in the youngest exhumed high- and ultrahigh-pressure terrane on Earth

Suzanne L. Baldwin[a,1], Jan Schönig[b], Joseph P. Gonzalez[a,2], Hugh Davies[c,3], and Hilmar von Eynatten[b]

[a]Department of Earth and Environmental Sciences, Syracuse University, Syracuse, NY 13244-1070; [b]Department of Sedimentology and Environmental Geology, University of Göttingen, D-37077 Göttingen, Germany; and [c]Geology Department, University of Papua New Guinea, Port Moresby 134, Papua New Guinea

Edited by Peter B. Kelemen, Lamont-Doherty Earth Observatory, Palisades, NY, and approved December 11, 2020 (received for review August 14, 2020)

Rock recycling within the forearcs of subduction zones involves subduction of sediments and hydrated lithosphere into the upper mantle, exhumation of rocks to the surface, and erosion to form new sediment. The compositions of, and inclusions within detrital minerals revealed by electron microprobe analysis and Raman spectroscopy preserve petrogenetic clues that can be related to transit through the rock cycle. We report the discovery of the ultrahigh-pressure (UHP) indicator mineral coesite as inclusions in detrital garnet from a modern placer deposit in the actively exhuming Late Miocene–Recent high- and ultrahigh-pressure ((U)HP) metamorphic terrane of eastern Papua New Guinea. Garnet compositions indicate the coesite-bearing detrital garnets are sourced from felsic protoliths. Carbonate, graphite, and CO_2 inclusions also provide observational constraints for geochemical cycling of carbon and volatiles during subduction. Additional discoveries include polyphase inclusions of metastable polymorphs of SiO_2 (cristobalite) and K-feldspar (kokchetavite) that we interpret as rapidly cooled former melt inclusions. Application of elastic thermobarometry on coexisting quartz and zircon inclusions in six detrital garnets indicates elastic equilibration during exhumation at granulite and amphibolite facies conditions. The garnet placer deposit preserves a record of the complete rock cycle, operative on <10-My geologic timescales, including subduction of sedimentary protoliths to UHP conditions, rapid exhumation, surface uplift, and erosion. Detrital garnet geochemistry and inclusion suites from both modern sediments and stratigraphic sections can be used to decipher the petrologic evolution of plate boundary zones and reveal recycling processes throughout Earth's history.

rock cycle | detrital garnet | ultrahigh-pressure metamorphism | Papua New Guinea

Throughout Earth's history, igneous, metamorphic, and sedimentary rocks have been recycled from the surface to upper mantle depths and subsequently returned as a result of tectonic and sedimentary processes operating within and at the surface of lithospheric plates. In active plate boundary zones, where most igneous and metamorphic rocks form, the rock cycle involves localized lithospheric deformation, which exhumes rocks to the Earth's surface. When rock exhumation occurs at plate tectonic rates (centimeters $year^{-1}$) (1, 2), high- and ultrahigh-pressure ((U)HP) metamorphic rocks containing hydrous mineral assemblages, trapped volatiles, and atmospheric gases (3, 4) may be returned from upper mantle depths to the surface in the forearcs of subduction zones. Mechanically strong host minerals, such as garnet, zircon, and clinopyroxene, and their nondecrepitated mineral inclusions have played a key role in the identification of (U)HP metamorphic rocks and conditions of metamorphism (5). After rocks are exposed at the surface, weathering processes erode (U)HP rocks to create sediment that is transported from source to sink, retaining evidence of metamorphic conditions in the compositions, and inclusions trapped within detrital mineral grains (6, 7). Garnet is a common mineral in metamorphic and igneous rocks of the upper mantle and crust that can survive transit through the rock cycle (8). Garnet is stable over a large range of pressure–temperature (P-T) conditions in many bulk rock compositions; commonly entraps and preserves (meta-)stable mineral inclusions; and is relatively resistant to chemical alteration during erosion, transport, and deposition. As a result, detrital garnet compositions (9) and their mineral inclusions (10), identified in the heavy-mineral fractions of sediments and sedimentary rocks, provide constraints on the conditions of garnet growth in source rocks.

The youngest known (U)HP terrane on Earth is actively exhuming in eastern Papua New Guinea within the obliquely convergent Australian (AUS)–Pacific (PAC) plate boundary zone (11) (Fig. 1). The Papuan (U)HP terrane formed when a rifted fragment of the Cretaceous AUS continental margin was subducted at the Aure–Pocklington trough (12, 13). In the D'Entrecasteaux Islands of the Woodlark Rift, Late Miocene–Recent metamorphic core complexes, composed of (U)HP metamorphic rocks (i.e., lower plate), have been exhumed to the surface at centimeters $year^{-1}$ rates from beneath upper plate rocks composed of oceanic lithosphere (14, 15). Direct evidence for ultrahigh-pressure (UHP) metamorphism has only been

Significance

On Earth, igneous, metamorphic, and sedimentary rocks are recycled from the surface to upper mantle depths and subsequently returned to the surface as a result of tectonic and sedimentary processes. Within active plate boundaries, the rock cycle involves lithospheric deformation to exhume rocks to the surface. We show that trapped inclusions in garnet sand from the actively exhuming high- and ultrahigh-pressure metamorphic terrane of eastern Papua New Guinea preserve a record of crustal subduction and rapid exhumation linking upper mantle and surface processes operative on short geologic timescales (<10 My). Detrital garnet geochemistry and their inclusion suites from both modern sediments and stratigraphic sections can be used to reveal rock recycling processes throughout Earth's history.

Author contributions: S.L.B. designed research; S.L.B. and H.D. led field expeditions to Papua New Guinea; and S.L.B., J.S., J.P.G., H.D., and H.v.E. performed research, analyzed data, and wrote the paper.

The authors declare no competing interest.

This article is a PNAS Direct Submission.

[1]To whom correspondence may be addressed. Email: sbaldwin@syr.edu.

[2]Present address: Department of Earth and Environmental Sciences, University of Pavia, 27100 Pavia, Italy.

[3]Present address: Research School of Earth Sciences, The Australian National University, Canberra, ACT 2000, Australia.

This article contains supporting information online at https://www.pnas.org/lookup/suppl/doi:10.1073/pnas.2017231118/-/DCSupplemental.

Published January 11, 2021.

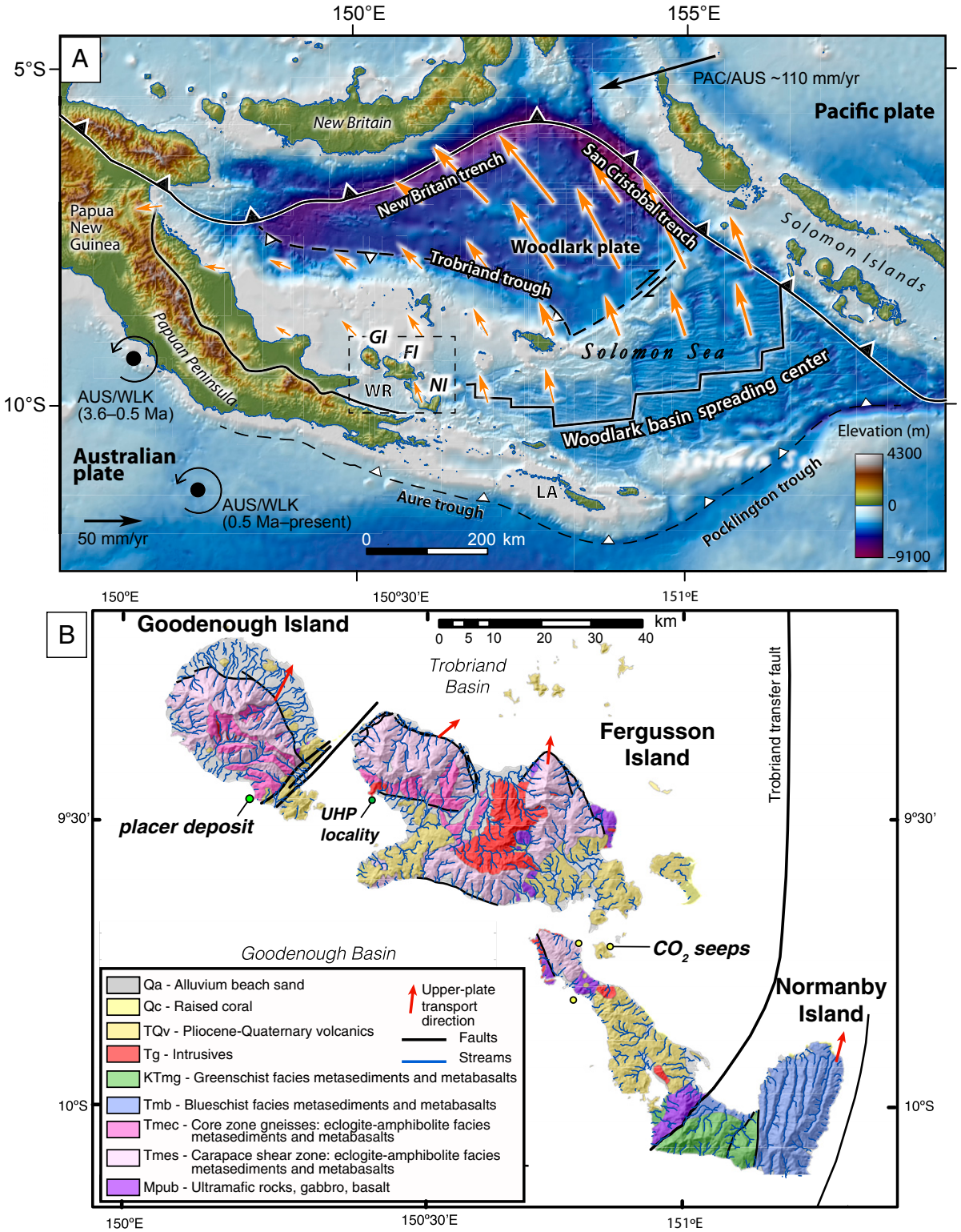

Fig. 1. (*A*) Tectonic and geologic setting of the (U)HP terrane in the Woodlark Rift of eastern Papua New Guinea. The (U)HP terrane is located within the larger obliquely convergent AUS–PAC plate boundary zone and formed when an AUS-derived continental fragment was subducted northward beneath oceanic lithosphere at the Aure–Pocklington trough. (U)HP rocks are found in the lower plates of metamorphic core complexes in the D'Entrecasteaux Islands (Goodenough Island [GI], Fergusson Island [FI], and Normanby Island [NI]), within the Woodlark Rift (WR). Low-grade metamorphic rocks of the accretionary wedge are exposed in the Louisiade Archipelago (LA). Global Positioning System model vectors (orange arrows) are shown for present-day Woodlark (WLK) plate motion relative to the AUS plate; AUS–WLK rotation poles for 3.6 to 0.5 Ma and 0.5 Ma to present are also indicated (50). Modified from ref. 19. (*B*) Geologic map of the D'Entrecasteaux Islands with the garnet placer deposit, coesite eclogite (UHP), and active CO_2 seep localities indicated. Base maps were made with GeoMapApp (51).

identified in one sample at one outcrop in the D'Entrecasteaux Islands (16). The coesite eclogite at this locality is interpreted to have formed ∼8 Ma when a partial mantle melt intruded subducted continental lithosphere at UHP conditions (4, 12, 17). Since the discovery of coesite eclogite, attempts to find additional mineral evidence for UHP metamorphism from outcrop samples, including from felsic lithologies, have been unsuccessful. However, intermediate-depth earthquakes in proximity to exhumed coesite eclogite indicate active seismicity in the tectonic setting where UHP exhumation is ongoing (18).

Goodenough Island, the westernmost metamorphic core complex within the subaerial portion of the Woodlark Rift, forms a prominent topographic dome where garnet-bearing eclogite and felsic to intermediate gneisses comprise a core zone and carapace shear zones (Fig. 1). Basement rocks include eclogite, granulite, and amphibolite with abundant evidence for in situ partial melts and granodioritic intrusions (Figs. 1 and 2). The dome is flanked by seismically active normal faults (18). Pliocene–Pleistocene surface uplift (19) and emergence of the islands above sea level led to erosion of the (U)HP terrane and deposition of Holocene colluvium and alluvium including the sampled garnet placer deposit, formed from erosion of garnet-bearing protoliths (Figs. 1*B* and 2*E*). Electron microprobe analysis and Raman spectroscopy of detrital garnets revealed evidence for rock recycling processes in the youngest exhumed (U)HP terrane on Earth where exhumation occurred during the same subduction cycle that produced the (U)HP rocks.

Results

The placer deposit contains (sub-)angular detrital garnet grains derived from a proximal source. Electron microprobe analyses of garnet from outcrop samples (compiled from the literature and this study) and detrital garnet (this study) allow a comparison of garnet compositions to assess potential sediment sources (Fig. 3 and *SI Appendix*). Ternary plots of garnet compositions (Fe + Mn, Ca, and Mg end-members) for crystalline rocks (n = 881) compared with detrital garnet compositions (n = 716) indicate that the detrital garnet grains cover the entire compositional range of potential crystalline source rocks.

Sixty-two percent of the detrital garnet grains investigated contained mineral inclusions. These include 83 garnets from the 63- to 125-μm-sized fraction, 117 garnets from the 125- to 200-μm-sized fraction, and 154 garnets from the >200-μm-sized fraction, with the largest grain having a long axis of ∼600 μm (*SI Appendix*). Detrital garnet mineral inclusions (≥2 μm) identified using Raman spectrometry include omphacite, kyanite, epidote, oxides (SiO_2 polymorphs, rutile), feldspars (alkali feldspar, plagioclase feldspar, kokchetavite), phyllosilicates (paragonite–muscovite series, phlogopite–biotite, chamosite–clinochlore, and pyrophyllite), and accessory phases (apatite, zircon, titanite) (Fig. 4 and *SI Appendix*). Rutile is the most abundant mineral inclusion, occurring in 73% of the inclusion-bearing detrital garnet grains studied. At least 2% of inclusion-bearing detrital garnets are inferred to be sourced from mafic eclogite as indicated by omphacite inclusions in high-Mg garnets (Fig. 3).

Three SiO_2 polymorphs (coesite, cristobalite, and quartz) were identified as inclusions in detrital garnets (Fig. 4). Quartz is the most abundant SiO_2 inclusion, occurring in 30% of the inclusion-bearing detrital garnets. Two garnets in the >200-μm fraction were sourced by UHP protoliths as indicated by a 4.0 × 3.0-μm polyphase SiO_2 inclusion, consisting of quartz and coesite (Fig. 4*A*), and a 6.5 × 5.5-μm monomineralic coesite inclusion (Fig. 4*B*). The garnet containing a polyphase coesite/quartz inclusion also contains carbonate, epidote, and CO_2 inclusions (Fig. 4*A*), whereas the monomineralic coesite inclusion coexists with numerous graphite inclusions in the same garnet grain (Fig. 4*B*).

Eleven detrital garnets contain cristobalite, the metastable highest-temperature polymorph of SiO_2. Raman spectra (Fig. 4*C*) indicate the inclusions are likely α-cristobalite (20). Nine (of 13) cristobalite crystals occur as polyphase inclusions, often together with mica (muscovite–paragonite, pyrophyllite, or chamosite–clinochlore) ± carbonate ± kokchetavite (Fig. 4*C* and *SI Appendix*). Kokchetavite, a metastable polymorph of K-feldspar (21), occurs in 4 of the 11 cristobalite-bearing garnets either in the same polyphase inclusion or as an adjacent inclusion. Five additional garnets were found to contain kokchetavite as polyphase inclusions (± quartz ± carbonate ± muscovite–paragonite ± rutile) (*SI Appendix*). The compositions of cristobalite- and kokchetavite-bearing garnet grains span the entire compositional range of the measured detrital garnets (Fig. 3).

Carbon-bearing inclusions consist of carbonate minerals (26% of inclusion-bearing garnets), graphite (22%), and CO_2 (19%) (Fig. 4 and *SI Appendix*). The compositions of carbon-bearing garnet grains also span the entire compositional range of the measured detrital garnets. However, graphite inclusions do not occur in high-Mg garnets. Therefore, we infer that carbon-bearing detrital garnets were derived from felsic sources (Fig. 3).

Six detrital garnets contained monomineralic elastically isolated quartz and zircon inclusions (i.e., away from grain boundaries, cracks, or other inclusions). The remnant strains of elastically isolated monomineralic quartz and zircon inclusions were used to constrain the P-T conditions of elastic equilibration within garnet hosts (Fig. 5). Application of elastic geothermobarometry requires that the inclusions remained isolated and fully contained within the host mineral after entrapment in order to preserve elastic strains from inclusion entrapment (22). However, inclusion strains can be modified through elastic, brittle, or ductile deformation (23–25), leading to modification of the calculated P-T conditions of elastic equilibration. Small (<10-μm-diameter) monomineralic inclusions contained within six detrital garnets from the >200-μm-size fraction were analyzed using Raman spectroscopy, ensuring that there is sufficient garnet volume to elastically isolate the inclusions (25–27) (*SI Appendix*). Each inclusion was verified to be more than three times the inclusion radii beneath the surface of the garnet and away from any visible inhomogeneities in the garnet host (i.e., other inclusions, fractures, or grain boundaries). The 1,008-cm^{-1} peak width, in terms of full width at half-maximum intensity, of less than 5 cm^{-1} was used as a criteria in the selection of nonmetamict zircon inclusions for Raman thermobarometry (27) (*SI Appendix*). Remnant strains were determined for quartz and zircon inclusions from measured Raman shifts using their respective Grüneisen tensor (28). No evidence of microfractures around inclusions was observed from visual inspection of each measured inclusion. Therefore, the remnant strains of the isolated inclusions within the garnet hosts are interpreted as the P-T conditions of elastic equilibration. Strains were used in conjunction with the elastic stiffness tensors of quartz and zircon to calculate the average remnant stress within the inclusions for use in an isotropic elastic model to constrain the range of possible elastic equilibration conditions [i.e., isomekes (29)]. P-T conditions of elastic equilibration between the host and inclusions were determined from the intersection points of isomekes calculated for coexisting quartz and zircon inclusions in six detrital garnets that met the criteria as stated above. Results indicate P-T conditions of elastic equilibration ranging from 0.5 to ∼1.3 GPa and from 550 °C to 750 °C. Despite the large uncertainties, the data suggest elastic equilibration under primarily granulite facies conditions and subordinate amphibolite facies conditions (Fig. 5).

Discussion

In the eastern Papuan (U)HP terrane outcrop samples of felsic gneisses that preserve UHP indicator minerals have yet to be found. Only one sample of mafic eclogite enclosed within retrogressed felsic gneiss has been found to preserve coesite as a partially transformed inclusion in omphacite (16). The coesite crystallized at 763 °C (+72 °C to −61 °C) and 3.3 GPa (+0.77 to −0.60 GPa) (30) during UHP metamorphism at ∼8 Ma (4, 17, 31) (Fig. 5). Garnet

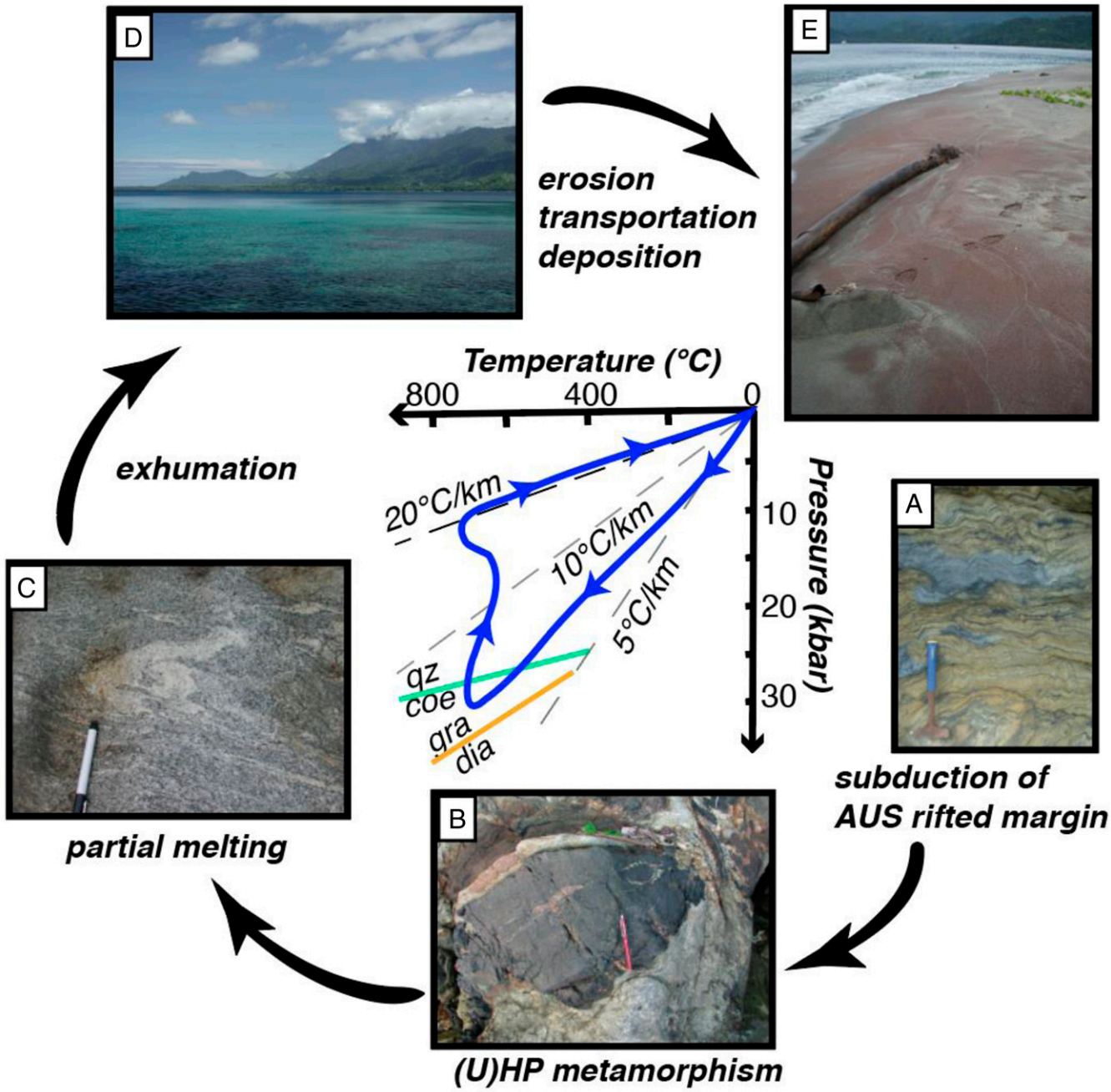

Fig. 2. Schematic figure illustrating rock (re-)cycling in the eastern Papuan (U)HP terrane where rifting of a subduction complex has exhumed (U)HP rocks since ∼8 Ma (i.e., negligible petrologic lag times). (*A*) Early–Middle Miocene northward subduction of an AUS continental fragment formed low-grade metamorphic rocks of the accretionary wedge [Calvados Schist, Louisiade archipelago (13)]. (*B*) (U)HP metamorphism of basalts and felsic protoliths formed eclogite in quartzofeldspathic host gneisses now exposed in the core zone, including in the catchment areas nearby the placer deposit locality. Coesite eclogite (UHP locality in Fig. 1*B*) formed at ∼8 Ma, whereas eclogite in the catchment area (in the photo) is as young as 2 Ma (31, 52). (*C*) Partial melting of gneisses in the garnet placer catchment area (in the photo), intrusion of igneous rocks, and volcanism have occurred since ∼4 Ma (14, 53). (*D*) Surface uplift to form the D'Entrecasteaux Islands since the Quaternary (19). (*E*) Rock erosion, transportation, and deposition of sediment to form a garnet-rich placer deposit. Schematic P-T path (details are presented in Fig. 5) illustrates conditions associated with metamorphic, igneous, and sedimentary rock formation and recycling in the Papuan (U)HP terrane. Geothermal gradients and reaction curves indicated (quartz [qz], coesite [coe], graphite [gra], and diamond [dia]).

growth in coesite eclogite occurred in two stages (32): 1) core garnet growth at ∼650 °C and >2.7 GPa within the coesite stability field and 2) garnet rim growth following partial exhumation from UHP conditions at <7.1 Ma during a transient (0.3-My) heating event at 1.5 GPa (Fig. 5).

Although it is not possible to extract the detailed P-T paths followed by individual detrital garnet grains, their compositions and inclusion suites can be compared with those from outcrop samples to assess the P-T paths followed by protoliths with a range of bulk compositions, during transit through the rock cycle (Figs. 3 and 5 and *SI Appendix*). The discovery of coesite inclusions in detrital garnets provides direct mineral evidence that UHP metamorphism also affected felsic lithologies in the eastern Papuan (U)HP terrane (Figs. 2–4). Compared with garnet from

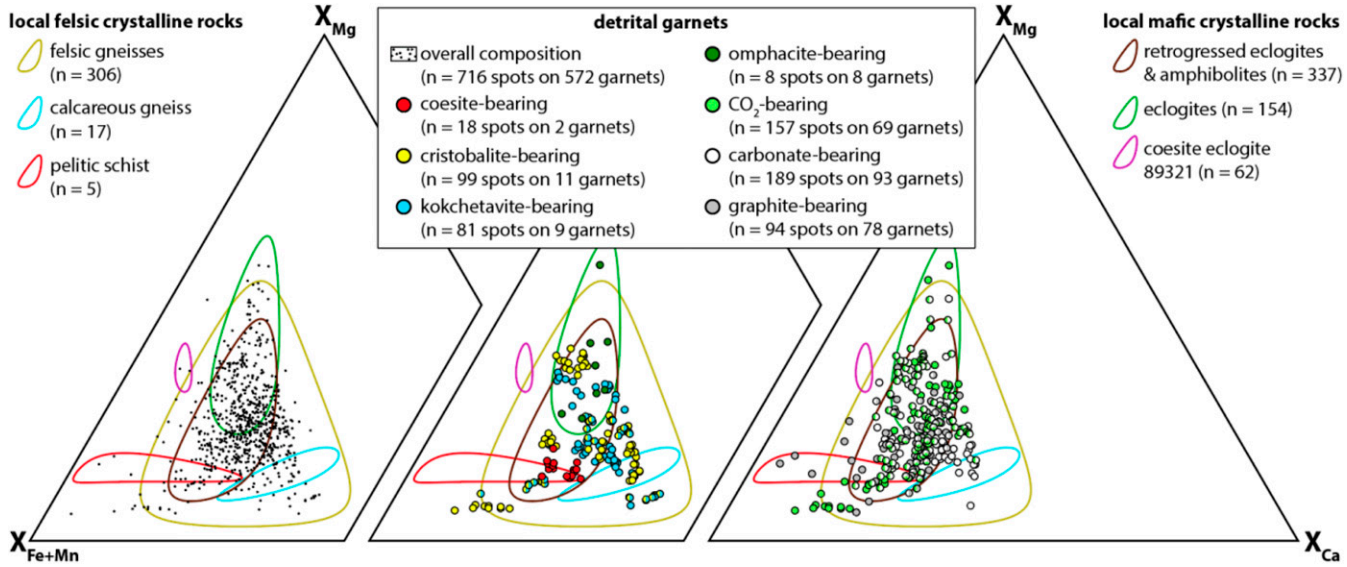

Fig. 3. Ternary plots of garnet compositions (molar proportions of Fe + Mn, Ca, and Mg) for metamorphic rocks of the lower plates of the D'Entrecasteaux Islands core complexes, as compared with detrital garnet compositions from the placer deposit. Garnet compositions from metamorphic rocks are color coded according to their bulk composition and plotted with 90% confidence ellipsoids; data were compiled from refs. 16, 31, 32, 38, 54, and 55 and this study (*SI Appendix*). The field-labeled felsic gneisses (n = 306) include aluminous gneisses, silicic gneisses, and quartzofeldspathic gneisses (including 03118m and 03115). Superimposed on garnet compositional fields are detrital garnet compositions (this study). Compositions of all detrital garnets (n = 716 spots on 572 garnets) are shown in *Left*. Garnet compositions corresponding to specific inclusion suites are shown in *Center* (coesite, cristobalite, kokchetavite, omphacite) and *Right* (CO_2, carbonate, graphite), as indicated in the legend.

the coesite eclogite outcrop, the two coesite-bearing detrital garnets have lower Mg contents and contain carbon-bearing inclusions (i.e., graphite, carbonate minerals, CO_2). These detrital garnets are inferred to have formed from metamorphism of organic-rich sedimentary rocks (Fig. 3 and *SI Appendix*), providing petrologic evidence for subduction of protoliths originating at the Earth's surface. No microdiamonds were found as inclusions in detrital garnet. Therefore, protolith conditions are inferred to have reached the coesite stability field but not the stability field for diamond (Figs. 2 and 5). Our findings expand the range of bulk compositions, notably low-density bulk compositions (felsic gneiss and metasedimentary rocks), that preserve evidence for UHP conditions in eastern Papua New Guinea.

Many mineral inclusions in the placer deposit garnets are commonly found as matrix minerals in basement rocks of the D'Entrecasteaux Islands (e.g., eclogite, felsic host gneiss, and amphibolite). However, cristobalite and kokchetavite are discoveries that have not yet been documented in basement rocks. Preservation of hydrous phases in the gneisses and shear zones on Goodenough Island (i.e., peak phengite, retrograde muscovite, biotite and chlorite, serpentinite) and mica and fluid inclusions preserved in detrital garnet span the entire compositional range (Fig. 3 and *SI Appendix*). We infer that fluids affected all lithologies during transit through the rock cycle. In order to be preserved, metastable mineral inclusions (i.e., coesite, cristobalite, kokchetavite) must have remained isolated systems, trapped within mechanically strong garnet hosts during rapid exhumation. These metastable inclusions also remained insulated from fluids during erosion and transport of sediment from limited catchment areas and deposition to form the placer deposit.

Detrital garnet mineral inclusions sourced by subducted carbonates and organic materials include graphite, carbonate minerals, and CO_2. We infer that subducted carbonaceous material converted to graphite via rapid recrystallization and devolatilization (33). However, subducted carbonaceous material apparently did not reach sufficient depths to form diamond. The abundance of graphite and CO_2 inclusions (22 and 19% of inclusion-bearing garnets, respectively) provides evidence for deep carbon recycling in the subduction channel (34). At present, shallow seeps offshore Normanby and Dobu Islands are releasing CO_2 (>98%) and CH_4 (87 to 4,360 ppm) (35) (Fig. 1*B*), providing evidence for the return of recycled carbon to the oceans and atmosphere.

Evidence for high-temperature conditions occurs in detrital garnets of all compositions. Polyphase inclusions of cristobalite + kokchetavite + mica (Fig. 4*C*) are interpreted as trapped partial melt crystallized during rapid decompression (i.e., "nanogranitoids") (36, 37) (*SI Appendix*). Elastic thermobarometry of individual detrital garnet grains also suggests elastic equilibration of quartz and zircon inclusions under granulite facies conditions and for one grain in the amphibolite facies (Fig. 5). Such high thermobaric ratios (T/P) are not compatible with equilibration along a prograde path associated with low-T/P subduction gradients but instead, provide additional evidence for heating during exhumation.

Although we are unable to ascertain the potential effects of chemical variations in quartz and zircon inclusions in the detrital garnets used for elastic thermobarometry, we found no evidence for elastic equilibration of quartz and zircon inclusions in detrital garnet corresponding to eclogite facies conditions. Instead, consistent P-T conditions in the high-temperature, lower-pressure metamorphic facies are obtained and cannot be attributed to processes that would variably affect individual inclusions, such as changes in the degree of elastic isolation or brittle deformation of inclusions. Therefore, we infer that the elastically isolated quartz and zircon inclusions in detrital garnets reequilibrated by viscous creep in their garnet hosts at temperatures >600 °C (25). Amphibolite facies conditions determined for one detrital garnet (DG-35) provide additional evidence for retrograde garnet growth, in agreement with quartz-in-garnet and Ti-in-quartz thermobarometry for a quartzofeldspathic gneiss in the catchment area (38) (Fig. 5).

The formation and preservation of both coesite and cristobalite as inclusions in garnet require extreme metamorphic conditions indicative of transient geothermal gradients (i.e., from low T/P to higher T/P). The rock record in eastern Papua New Guinea preserves evidence for Late Miocene low-T/P metamorphism reaching UHP conditions and higher-T/P metamorphism during exhumation, as well as highest-T/P gradients

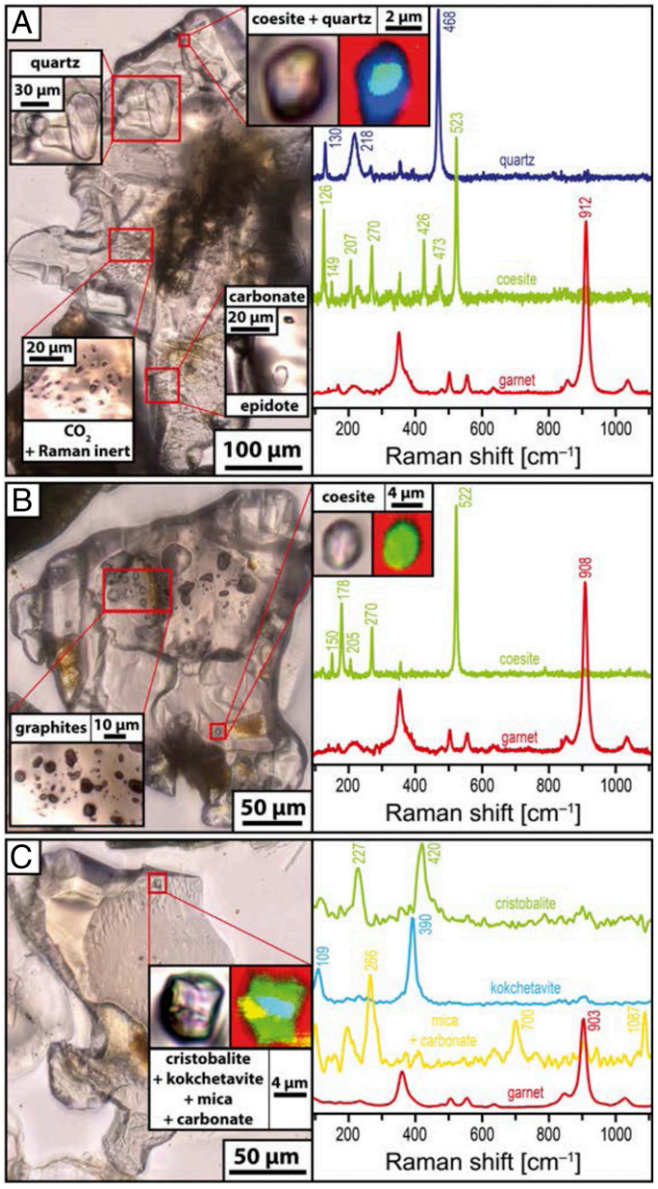

Fig. 4. Representative detrital garnets and inclusion suites and associated Raman spectra. (*A*) Detrital garnet containing polyphase quartz and coesite, carbonate, epidote, and CO_2 inclusions. (*B*) Detrital garnet containing monomineralic coesite and graphite inclusions. (*C*) Detrital garnet containing a polyphase inclusion of cristobalite + kokchetavite + mica + carbonate.

associated with decompression melting of asthenospheric mantle to form basalts in the Woodlark Basin (Figs. 1 and 2). The UHP locality occurs along strike of a sinistral strike–slip transfer fault system from the placer deposit (39); the faults displace Pliocene–Quaternary basaltic lavas (Fig. 1*B*). Such petrologic variation preserved in the geologic record over short spatial and temporal scales indicates that steady-state processes are not operative within this part of the obliquely convergent AUS–PAC plate boundary zone (11).

The detrital garnet data support models for the transport and transformation pathways of heterogeneous lithologies, including organic and inorganic carbon, in the forearcs of subduction zones (34). Results reinforce the observation that subducted rocks do not have to remain dry during transport through the rock cycle in order to preserve evidence for UHP metamorphism, as long as mineral inclusions (such as coesite) in strong host minerals, like garnet, remain isolated from metamorphic fluids (5). In addition, detrital garnet data provide observational evidence for H_2O and CO_2 storage in the forearc and volatile and melt migration within the forearc during rifting. We infer that the detrital garnet SiO_2 inclusions (coesite, quartz, and cristobalite) capture processes including subduction to upper mantle depths along low-T/P gradients and exhumation associated with an increase in geothermal gradients (i.e., to higher T/P) as the Woodlark Rift formed ahead of the westward-propagating Woodlark Basin seafloor-spreading system (Fig. 1*A*).

The Papuan (U)HP terrane preserves evidence for geochemical cycling between the surface and the upper mantle, including UHP rock formation and exhumation, that can be directly linked to the rapid spatial and temporal evolution of the obliquely convergent PAC–AUS plate boundary zone. Microplate rotation of the Woodlark plate relative to the AUS plate (40), upper plate divergence (41), and buoyancy forces (42) contributed to rapid (U)HP exhumation during the transition from subduction to rifting in eastern Papua New Guinea (Fig. 1). Following the onset of upper plate divergent motion, the oceanic upper plate and subducted continental lower plate will decouple, providing accommodation space (41) for subducted metasediments, felsic gneisses, and their partial melts to rapidly exhume within the subduction channel. Numerical models that use constraints provided by the geologic record in eastern Papua New Guinea (43, 44) predict that asthenospheric mantle will flow upward toward the subduction channel to fill the accommodation space left by the buoyantly exhuming felsic (U)HP rocks, resulting in isotherm advection, an increase in geothermal gradients, and heating of the (U)HP terrane during exhumation.

The investigation of erosional products at the catchment scale expands the potential for finding additional evidence of UHP metamorphism in the eastern Papuan (U)HP terrane where pervasively overprinted felsic rocks and their partial melts have

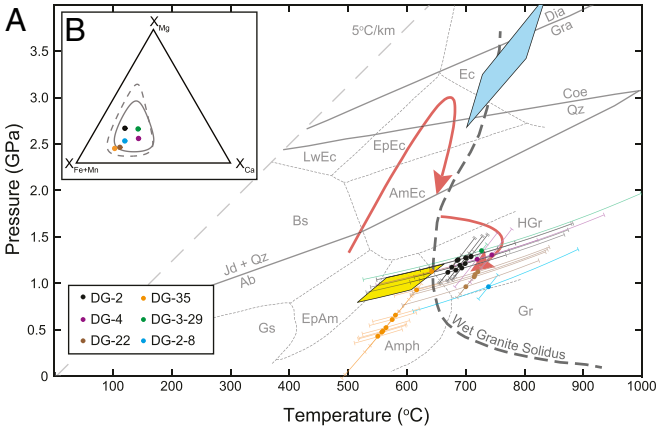

Fig. 5. P-T diagram showing (*A*) quartz-in-garnet and zircon-in-garnet elastic thermobarometric data for detrital garnets (DGs; this study). Also shown are P-T constraints for outcrop samples, including quartzofeldspathic gneiss in the catchment area [sample 03115; yellow field (38)]. P-T path (red arrows) was derived from garnet compositions from coesite eclogite (32). Blue field indicates Ti-in-coesite trace element thermobarometry, combined with zirconium-in-rutile thermometry for coesite eclogite (30, 56). (*B*) Ternary plot of detrital garnet compositions (molar proportions of Fe + Mn, Ca, and Mg) corresponding to the quartz-in-garnet and zircon-in-garnet elastic thermobarometric data plotted in *A*. The solid line indicates the 90% confidence ellipsoids for all detrital garnet grains, and the dashed line is the 90% confidence ellipsoid for all garnet compositions from basement rocks. Coe, coesite; Dia, diamond; Gra, graphite; Qz, quartz; Jd, jadeite; Ab, albite. Metamorphic facies indicated: Ec, eclogite; EpEc, epidote eclogite; AmEc, amphibole eclogite; LwEc, lawsonite eclogite; Bs, blueschist; Gs, greenschist; EpAm, epidote amphibolite; Amph, amphibolite; Gr, granulite; HGr, high-pressure granulite.

yet to yield additional evidence in outcrop since coesite was discovered in a mafic eclogite. Results demonstrate that inclusions in detrital garnets from modern sediments preserve evidence for UHP metamorphism. Such geologically short timescales (i.e., since the Late Miocene) for rock recycling within this active plate boundary zone imply <10-My petrologic lag times for metamorphic rocks exhumed from approximately ≤120-km depths, eroded, and deposited as sediment. High-spatial resolution spectroscopic imaging of heavy mineral fractions of sediment derived from the erosion of the Papuan (U)HP terrane provides a means to efficiently search for evidence of UHP metamorphism and to further constrain the thermal evolution and geodynamics of continental subduction. A better understanding of subduction and exhumation processes in active plate boundaries is needed before modern processes can be accurately extrapolated and applied to the geologic record. Raman spectroscopy of mineral inclusions in detrital garnet in both modern sediments and stratigraphic sections, especially when integrated with single-grain Sm–Nd detrital garnet ages (45), has the potential to provide insight into the tempo of rock recycling processes throughout Earth's history, including on early Earth when plate velocities and transport through the rock cycle were at least as fast as present day.

Materials and Methods

The beach placer sample (PNG08002c) was dry sieved into sized fractions (63 to 125, 125 to 200, and >200 μm), split by coning and quartering, mounted in epoxy, ground with SiC, and polished with Al_2O_3 to expose grain surfaces. The compositions of 572 detrital garnet grains were obtained by electron microprobe analysis at the Geosciences Center of the University of Göttingen using a JEOL JXA 8900 RL equipped with five wavelength dispersive spectrometers. Measurements were performed with an accelerating voltage 15 kV and a beam current of 20 nA. Counting times were 15 s for Si, Mg, Ca, Fe, and Al and 30 s for Ti, Cr, and Mn. Measurement spots were preferentially set to the garnet centers but shifted toward the rim when inclusions or fractures are located in the center. For the coesite-, cristobalite-, and kokchetavite-bearing garnet grains, nine spots per garnet were set: one at the center, four at the mantle, and four at the rim.

From the investigated 572 garnet grains, 354 contain inclusions ≥2 μm, which were identified using a Horiba Jobin Yvon XploRA Plus spectrometer equipped with an Olympus BX41 microscope at the Geosciences Center of the University of Göttingen (10). Analytical conditions include a 532-nm excitation laser, a 1,800-L mm^{-1} grating, a 100× long working distance objective with a numerical aperture of 0.8, a confocal hole diameter of 100 μm, and a slit of 100 μm. Two-dimensional Raman images of monomineralic coesite, bimineralic coesite/quartz, and polyphase inclusions containing cristobalite and kokchetavite were collected with a WITec alpha300R ultrahigh-throughput Raman spectrometer at the Geosciences Center of the University of Göttingen. The spectral images were acquired with a 532-nm excitation laser, an automatically controlled laser power of 20 mW, a 1,200-L mm^{-1} grating, and a 100× long working distance objective with a numerical aperture of 0.75. Spectra were collected at a step size of between 50 and 200 nm using an acquisition time of between 1 and 2 s per spectrum, depending on the specific inclusion. Automated cosmic ray correction, background subtraction, spectral averaging/smoothing, and supervised component analysis were performed using the WITec Project software.

A Renishaw inVia Raman spectrometer with a confocal optical microscope at Syracuse University was used to measure the Raman shifts of quartz and zircon inclusions in detrital garnet for elastic thermobarometric calculations following procedures for quartz-in-garnet inclusions (38, 46) and zircon-in-garnet inclusions (27). All measured inclusions were elastically isolated and located more than three inclusion radii from other inclusions, grain boundaries, and visible defects in the host garnet. Because metamictization of zircon modifies the zircon bulk elastic properties (27), only nonmetamict zircon inclusions were selected for analysis as determined using the 1,008-cm^{-1} peak width, in terms of full width at half-maximum (FWHM) intensity, of less than 5 cm^{-1} (*SI Appendix*). A 532-nm laser was focused onto specimens with a 100× microscope objective with a numerical aperture of 0.9. The Raman scattered light was statically dispersed with a 1,800-L mm^{-1} grating onto a charged couple device, resulting in a spectral resolution of 0.5 cm^{-1}. The spectrometer was calibrated against neon lines and a silicon standard. Spectral accuracy and linearity were checked throughout each analytical session by measuring the Rayleigh scattered light from the 532-nm laser, the 520.5-cm^{-1} Raman band of a silicon standard, the Raman bands of a synthetic quartz reference material from the Westinghouse Corporation, and the Raman bands of a synthetic zircon reference material. All Raman spectra were acquired for 20 s and measured at room conditions of 23 °C and 1 bar. Spectra were not processed or corrected prior to peak fitting using a pseudo-Voigt function in the Renishaw software. Errors on fitted band positions are ∼0.2 to 0.3 cm^{-1}.

For strain calculations, Raman band frequencies of quartz were measured at ∼127.5, 205.9, and 464.8 cm^{-1}, and the Raman band frequencies of zircon were measured at 213.4, 224.0, 356.0, 438.8, 974.8, and 1,008.7 cm^{-1}. Synthetic quartz and zircon reference materials were measured between sample measurements to derive calibration curves in the case of any spectral drift. Measurements were performed near the centers of the inclusions, where the effects of inclusion geometry and elastic anisotropy have the least effect (26). Furthermore, it has recently been demonstrated that when elastically anisotropic inclusions, such as quartz and zircon, are contained within nearly isotropic host minerals such as garnet, the effect of elastic anisotropy on calculated entrapment conditions is <2% and therefore, negligible as compared with the errors on Raman measurements (47). The remnant strains ($\varepsilon_1 + \varepsilon_2$, ε_3) in inclusions were calculated using the fitted Raman band positions using the stRAinMAN software and the respective Grüneisen tensors of quartz and zircon (28). Errors on fitted band positions of 0.3 cm^{-1} were used in stRAinMAN to calculate the estimated standard deviation (esd) and covariance matrix needed for error calculation of the remnant inclusion pressure (48). Remnant strains of quartz and zircon inclusions were used in conjunction with the respective elastic tensor to calculate the pressure within the inclusion. Elastic modeling of inclusion pressures and entrapment isomekes was performed for quartz and zircon inclusions in an almandine host using an isotropic elastic model implemented in the EntraPT program (49). Errors on remnant strains were propagated to entrapment isomekes using the covariance matrix and esd on inclusion strains according to the method described in ref. 49. Errors on calculated entrapment isomekes, especially for zircon inclusions in garnet, varied over a large temperature range. Inclusions with the largest errors were those that had the least number of fitted Raman bands and were subsequently excluded from P-T calculations and interpretation.

Data Availability. All study data are included in the article and supporting information.

ACKNOWLEDGMENTS. S.L.B. acknowledges support from NSF Division of Earth Sciences Grant 0709054, NSF Major Research Instrumentation Program Grant 1625835, and the Thonis Endowment at Syracuse University. J.S. and H.v.E. acknowledge support from German Research Foundation Grant EY 23/27-1. J.P.G. acknowledges support from a Syracuse University Science Technology Engineering Math fellowship and a European Research Council Postdoctoral Fellowship (Grant 714936 to M. Alvaro). We thank R. M. Davies for garnet electron microprobe analyses and P. G. Fitzgerald for providing comments on an earlier version of the manuscript. We acknowledge the constructive reviews of Editor Peter Kelemen and two anonymous reviewers, which helped us improve our manuscript. Collaborative discussions on detrital analysis with S. Andò, M .G. Malusà, E. Garzanti, and P. G. Fitzgerald are greatly appreciated.

1. D. Rubatto, J. Hermann, Exhumation as fast as subduction? *Geology* **29**, 3–6 (2001).
2. S. L. Baldwin *et al.*, Pliocene eclogite exhumation at plate tectonic rates in eastern Papua New Guinea. *Nature* **431**, 263–267 (2004).
3. G. E. Bebout, S. C. Penniston-Dorland, Fluid and mass transfer at subduction interfaces—the field metamorphic record. *Lithos* **240–243**, 228–258 (2016).
4. S. L. Baldwin, J. P. Das, Atmospheric Ar and Ne returned from mantle depths to the Earth's surface by forearc recycling. *Proc. Natl. Acad. Sci. U.S.A.* **112**, 14174–14179 (2015).
5. S. Ferrero, R. J. Angel, Micropetrology: Are inclusions grains of truth? *J. Petrol.* **59**, 1671–1700 (2018).
6. J. Schönig, G. Meinhold, H. von Eynatten, N. K. Lünsdorf, Tracing ultrahigh-pressure metamorphism at the catchment scale. *Sci. Rep.* **8**, 2931 (2018).
7. J. Schönig, H. von Eynatten, G. Meinhold, N. K. Lünsdorf, Diamond and coesite inclusions in detrital garnet of the Saxonian Erzgebirge, Germany. *Geology* **47**, 715–718 (2019).
8. E. F. Baxter, M. J. Caddick, J. J. Ague, Garnet: Common mineral, uncommonly useful. *Elements* **9**, 415–419 (2013).
9. M. A. Mange, A. C. Morton, "Geochemistry of heavy minerals" in *Developments in Sedimentology*, M. A. Mange, D. T. Wright, Eds. (Elsevier, 2007), vol. 58, pp. 345–391.
10. J. Schönig, G. Meinhold, H. von Eynatten, N. K. Lünsdorf, Provenance information recorded by mineral inclusions in detrital garnet. *Sediment. Geol.* **376**, 32–49 (2018).

11. S. L. Baldwin, P. G. Fitzgerald, L. E. Webb, Tectonics of the New Guinea region. *Annu. Rev. Earth Planet. Sci.* **40**, 495–520 (2012).
12. N. A. Zirakparvar, S. L. Baldwin, J. D. Vervoort, The origin and geochemical evolution of the Woodlark Rift of Papua New Guinea. *Gondwana Res.* **23**, 931–943 (2013).
13. L. E. Webb, S. L. Baldwin, P. G. Fitzgerald, The early-middle Miocene subduction complex of the Louisiade archipelago, southern margin of the Woodlark Rift. *Geochem. Geophys. Geosyst.* **15**, 4024–4046 (2014).
14. S. L. Baldwin, G. S. Lister, E. J. Hill, D. A. Foster, I. McDougall, Thermochronologic constraints on the tectonic evolution of active metamorphic core complexes, D'Entrecasteaux Islands, Papua New Guinea. *Tectonics* **12**, 611–628 (1993).
15. T. A. Little, S. L. Baldwin, P. G. Fitzgerald, B. Monteleone, Continental rifting and metamorphic core complex formation ahead of the Woodlark spreading ridge, D'Entrecasteaux Islands, Papua New Guinea. *Tectonics* **26**, TC1002 (2007).
16. S. L. Baldwin, L. E. Webb, B. D. Monteleone, Late Miocene coesite-eclogite exhumed in the Woodlark Rift. *Geology* **36**, 735–738 (2008).
17. N. A. Zirakparvar, S. L. Baldwin, J. D. Vervoort, Lu–Hf garnet geochronology applied to plate boundary zones: Insights from the (U)HP terrane exhumed within the Woodlark Rift. *Earth Planet. Sci. Lett.* **309**, 56–66 (2011).
18. G. A. Abers *et al*., Southeast Papuan crustal tectonics: Imaging extension and buoyancy of an active rift. *J. Geophys. Res. Solid Earth* **121**, 951–971 (2016).
19. S. R. Miller, S. L. Baldwin, P. G. Fitzgerald, Transient fluvial incision and active surface uplift in the Woodlark Rift of eastern Papua New Guinea. *Lithosphere* **4**, 131–149 (2012).
20. I. P. Swainson, M. T. Dove, D. C. Palmer, Infrared and Raman spectroscopy studies of the alpha phase transition in cristobalite. *Phys. Chem. Miner.* **30**, 353–365 (2003).
21. S.-L. Hwang *et al*., Kokchetavite: A new potassium-feldspar polymorph from the kokchetav ultrahigh-pressure terrane. *Contrib. Mineral. Petrol.* **148**, 380–389 (2004).
22. R. J. Angel, P. Nimis, M. L. Mazzucchelli, M. Alvaro, F. Nestola, How large are departures from lithostatic pressure? Constraints from host-inclusion elasticity. *J. Metamorph. Geol.* **33**, 801–813 (2015).
23. N. Campomenosi *et al*., How geometry and anisotropy affect residual strain in host inclusion system: Coupling experimental and numerical approaches. *Am. Mineral.* **103**, 1–15 (2018).
24. M. Alvaro *et al*., Fossil subduction recorded by quartz from the coesite stability field. *Geology* **48**, 24–28 (2020).
25. X. Zhong, E. Moulas, L. Tajčmanová, Post-entrapment modification of residual inclusion pressure and its implications for Raman elastic thermobarometry. *Solid Earth* **11**, 223–240 (2020).
26. M. L. Mazzucchelli *et al*., Elastic geothermobarometry: Corrections for the geometry of the host-inclusion system. *Geology* **46**, 231–234 (2018).
27. N. Campomenosi *et al*., Establishing a protocol for the selection of zircon inclusions in garnet for Raman thermobarometry. *Am. Mineral.* **105**, 992–1001 (2020).
28. R. J. Angel, M. Murri, B. Mihailova, M. Alvaro, Stress, strain and Raman shifts. *Z. Kristallogr. Cryst. Mater.* **234**, 129–140 (2019).
29. R. J. Angel, M. L. Mazzucchelli, M. Alvaro, F. Nestola, EosFit-pinc: A simple GUI for host-inclusion elastic thermobarometry. *Am. Mineral.* **102**, 1957–1960 (2017).
30. Z. R. Osborne *et al*., An experimentally calibrated thermobarometric solubility model for titanium in coesite (TitaniC). *Contrib. Mineral. Petrol.* **174**, 34 (2019).
31. B. D. Monteleone *et al*., Late miocene-pliocene eclogite facies metamorphism, D'Entrecasteaux Islands, SE Papua New Guinea. *J. Metamorph. Geol.* **25**, 245–265 (2007).
32. S. W. Faryad, S. L. Baldwin, R. Jedlicka, J. Ježek, Two-stage garnet growth in coesite eclogite from the southeastern Papua New Guinea (U)HP terrane and its geodynamic significance. *Contrib. Mineral. Petrol.* **174**, 73 (2019).
33. Y. Nakamura, T. Yoshino, M. Satish-Kumar, Pressure dependence of graphitization: Implications for rapid recrystallization of carbonaceous material in a subduction zone. *Contrib. Mineral. Petrol.* **175**, 32 (2020).
34. M. Galvez, M. Pubellier, "How do subduction zones regulate the carbon cycle?" in *Deep Carbon: Past to Present*, B. Orcutt, I. Daniel, R. Dasgupta, Eds. (Cambridge University Press, 2019), pp. 276–312.
35. K. E. Fabricius *et al*., Losers and winners in coral reefs acclimatized to elevated carbon dioxide concentrations. *Nat. Clim. Chang.* **1**, 165–169 (2011).
36. S. Ferrero, M. A. Ziemann, R. J. Angel, P. J. O'Brien, B. Wunder, Kumdykolite, kokchetavite, and cristobalite crystallized in nanogranites from felsic granulites, Orlica-Snieznik Dome (Bohemian Massif): Not evidence for ultrahigh-pressure conditions. *Contrib. Mineral. Petrol.* **171**, 3 (2016).
37. J. Schönig *et al*., Deep subduction of felsic rocks hosting UHP lenses in the central Saxonian Erzgebirge: Implications for UHP terrane exhumation. *Gondwana Res.* **87**, 320–329 (2020).
38. J. P. Gonzalez, J. B. Thomas, S. L. Baldwin, M. Alvaro, Quartz-in-garnet and Ti-in-quartz thermobarometry: Methodology and first application to a quartzofeldspathic gneiss from eastern Papua New Guinea. *J. Metamorph. Geol.* **37**, 1193–1208 (2019).
39. E. J. Hill, Geometry and kinematics of shear zones formed during continental extension in eastern Papua New Guinea. *J. Struct. Geol.* **16**, 1093–1105 (1994).
40. L. E. Webb, S. L. Baldwin, T. A. Little, P. G. Fitzgerald, Can microplate rotation drive subduction inversion. *Geology* **36**, 823–826 (2008).
41. M. G. Malusà *et al*., Contrasting styles of (U)HP rock exhumation along the cenozoic adria-Europe plate boundary (Western Alps, Calabria, Corsica). *Geochem. Geophys. Geosyst.* **16**, 1786–1824 (2015).
42. S. M. Ellis, T. A. Little, L. M. Wallace, B. R. Hacker, S. J. H. Buiter, Feedback between rifting and diapirism can exhume ultrahigh-pressure rocks. *Earth Planet. Sci. Lett.* **311**, 427–438 (2011).
43. K. D. Petersen, W. R. Buck, Eduction, extension, and exhumation of ultrahigh-pressure rocks in metamorphic core complexes due to subduction initiation. *Geochem. Geophys. Geosyst.* **16**, 2564–2581 (2015).
44. J. Liao *et al*., Divergent plate motion drives rapid exhumation of (ultra)high pressure rocks. *Earth Planet. Sci. Lett.* **491**, 67–80 (2018).
45. K. A. Maneiro, E. F. Baxter, S. D. Samson, H. R. Marschall, J. Hietpas, Detrital garnet geochronology: Application in tributaries of the French Broad River, Southern Appalachian Mountains, USA. *Geology* **47**, 1189–1192 (2019).
46. M. Bonazzi, S. Tumiati, J. B. Thomas, R. J. Angel, M. Alvaro, Assessment of the reliability of elastic geobarometry with quartz inclusions. *Lithos* **350–351**, 105201 (2019).
47. M. L. Mazzucchelli, A. Reali, S. Morganti, R. J. Angel, M. Alvaro, Elastic geobarometry for anisotropic inclusions in cubic hosts. *Lithos* **350–351**, 105218 (2019).
48. R. J. Angel, M. Alvaro, R. Miletich, F. Nestola, A simple and generalised P–T–V EoS for continuous phase transitions, implemented in EosFit and applied to quartz. *Contrib. Mineral. Petrol.* **172**, 29 (2017).
49. M. L. Mazzucchelli, R. J. Angel, M. Alvaro, Entra PT: An online application for elastic geothermobarometry. *Am. Mineral*, http://www.minsocam.org/MSA/Ammin/AM_Preprints/7693MazzucchelliPreprint.pdf.
50. L. M. Wallace *et al*., GPS and seismological constraints on active tectonics and arc-continent collision in Papua New Guinea: Implications for mechanics of microplate rotations in a plate boundary zone. *J. Geophys. Res.* **109**, B05404 (2004).
51. W. B. F. Ryan *et al*., Global multi-resolution topography synthesis. *Geochem. Geophys. Geosyst.* **10**, Q03014 (2009).
52. N. A. Zirakparvar, S. L. Baldwin, A. K. Schmitt, Zircon growth in (U)HP quartzo-feldspathic host gneisses exhumed in the Woodlark Rift of Papua New Guinea. *Geochem. Geophys. Geosyst.* **15**, 1258–1282 (2014).
53. S. M. Gordon *et al*., Multi-stage exhumation of young UHP–HP rocks: Timescales of melt crystallization in the D'Entrecasteaux Islands, southeastern Papua New Guinea. *Earth Planet. Sci. Lett.* **351–352**, 237–246 (2012).
54. H. L. Davies, R. G. Warren, Eclogites of the D'Entrecasteaux Islands. *Contrib. Mineral. Petrol.* **112**, 463–474 (1992).
55. J. W. DesOrmeau, S. M. Gordon, T. A. Little, S. A. Bowring, N. Chatterjee, Rapid time scale of Earth's youngest known ultrahigh-pressure metamorphic event, Papua New Guinea. *Geology* **45**, 795–798 (2017).
56. M. J. Kohn, A refined zirconium-in-rutile thermometer. *Am. Mineral.* **105**, 963–971 (2020).